Bioelectrochemistry 155 (2024) 108597

Contents lists available at ScienceDirect

Bioelectrochemistry

journal homepage: www.journals.elsevier.com/bioelectrochemistry

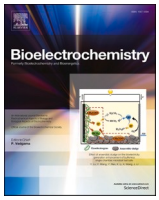

Evaluation of a comprehensive power management system with maximum power point tracking algorithm for multiple microbial fuel cell energy harvesting

Rodrigo Fernandez Feito *, Tahreem Younas, Richard M. Dinsdale

Sustainable Environment Research Centre, University of South Wales, Llantwit Road, Pontypridd, Rhondda Cynon Taff CF37 1DL, UK

ARTICLE INFO

Keywords:
Microbial fuel cells
Maximum power point tracking
Power management system
Energy harvesting
Series and parallel connection

ABSTRACT

This study presents a comprehensive power management system (PMS) capable of tracking the maximum power point (MPP) and harvesting the energy from up to five microbial fuel cells (MFCs). The harvested energy from the MFCs was used to power the electronics, and in cases where this power was insufficient, alternative backup power options can be used. The voltage can be increased up to 3.3 V, and a hysteresis-based control approach was utilised to regulate the output voltage. The MPP of each MFC was determined using a variable step size incremental conductance algorithm that controls the duty cycle of the synchronous boost converters. No additional electronic components are necessary for the operation of the N and P-channel MOSFETs. The efficiency of the PMS relies on the target output voltage and the power output characteristics of the MFCs. Efficiencies of up to 87 % were achieved by combining the outputs of each MFC boost converter. To save energy, some electronic components are disabled when not in use, and the maximum power consumption of the PCB is below 5.8 mW at an output voltage of 3.3 V. The PMS is applied to simulated and real tubular MFCs under various operating conditions.

1. Introduction

The research on Microbial Fuel Cell (MFC) technology has gained significant attention in recent times due to its potential in addressing energy and environmental concerns. This approach combines waste treatment and electricity generation [1,2], making it a promising solution for achieving sustainable energy and environmental practices. MFCs are particularly interesting for remote sensing [3,4], pollution control [5] and energy production [6,7]. MFCs serve as a sustainable energy option, wherein electricity is produced by bacteria residing within a reactor. These bacteria harness electrons from biodegradable materials present in the anode chamber and subsequently transfer them to the anode electrode. The electrons follow a path from the anode through an external circuit to the cathode, where they contribute to the reduction of an electron acceptor, like oxygen.

The flow of electrons from the anode to the cathode can be harnessed to perform mechanical or electrical work. Typically, in most of the research conducted, MFCs are utilized with fixed external resistances or applied potentials. Consequently, power density estimates are determined through polarization curves, assuming that the highest power density is attained when the external resistance matches the MFC's internal resistance [8,9,10,11]. While these descriptions do illustrate the theoretical capabilities of MFCs in terms of power production, the generated electricity is not effectively utilized as it is predominantly transformed into thermal energy instead. In addition, achieving the highest power output in MFC operation is not always possible due to the inability of a fixed external resistance to consistently align with the system's internal resistance. The internal resistance of an MFC fluctuates continuously due to variations in microbial activities and operational factors like substrate concentration, pH, and temperature [12,13].

To harvest the MFC energy efficiently, the elimination of superfluous resistors is required. Moreover, MFCs produce low-voltage outputs that are inadequate to power integrated circuits, sensors, and pumps directly. Through the connection of the electrical circuits of MFCs in series, it is possible to increase the output voltage. However, this may result in voltage reversal, which typically arises when certain cells within the stack experience a more extreme voltage level than others. Voltage reversal manifests in the weakest performing cell, which subsequently becomes a parasitic load within the array, thereby reducing the output voltage of the stack and decreasing its overall efficiency [11,14,15]. The

* Corresponding author.
E-mail address: Rodrigo.fernandezfeito@southwales.ac.uk (R. Fernandez Feito).

https://doi.org/10.1016/j.bioelechem.2023.108597
Received 4 September 2023; Received in revised form 9 October 2023; Accepted 1 November 2023
Available online 3 November 2023

avoidance of voltage reversal can be achieved through the incorporation of a maximum power point tracking (MPPT) control [11,16]. Furthermore, when operating at the maximum power point (MPP), the removal of organic pollution as chemical oxygen demand (COD) is typically enhanced, while the output power is maximized [17,18].

An effective strategy for harnessing MFC power for real-world applications lies in the implementation of a power management system (PMS) [19,20,21]. Typically, a PMS consists of an electronic circuit comprised of various elements, including charge pumps, capacitors, inductors, step-up converters, power switches, diodes, and/or potentiometers [22]. The optimal utilization of MFCs depend significantly on the implementation of PMSs, which ideally should perform three essential tasks: (i) optimizing the power generation of MFCs by operating them at their MPP, (ii) efficiently capturing and storing the energy generated by the MFCs, and (iii) maintaining the output voltage within the desired range. Hence, power management systems are critical for enhancing the efficiency and effectiveness of MFCs.

The different PMSs reported so far are divided into two main groups, capacitor-based systems which use capacitors to boost the power output [23,24,25,26], or boost converter-based systems which use inductors to store energy momentarily and then this energy is released to step up the input voltage [27–44]. In recent times, considerable research has been conducted on the feasibility of utilizing commercially available boost converters and power management chips. However, most off-the-shelf boost converters typically demand an input voltage of at least 0.7 V, which surpasses the voltage output typically generated by most MFCs. There are a few exceptions like the LTC3108 and TPS612x converters [16,27–30]. The LTC3108 can function with a minimum input voltage of 20 mV, but its efficiency is limited to 30 % when input voltages exceed 0.2 V. On the other hand, the TPS612x requires a minimum input voltage of 0.3 V but consumes approximately 2 mW at this voltage, potentially utilizing all the power generated by most lab-scale MFCs. Moreover, the use of these devices makes does not allow the implementation of MPPT. Recently, the BQ25504 ultra-low power boost converter with MPPT capabilities has gained significant popularity in MFC applications [30–35]. This converter is capable of harvesting energy from low-input voltage sources as low as 130 mV and incorporates MPP harvesting functionality. However, the BQ25504′s 16-second open circuit measurement interval for 256 ms poses practical challenges for MFC MPPT due to their slow dynamics. Consequently, employing this feature could cause MFCs to operate significantly far from the MPP.

MPPT in MFCs involves dynamically adjusting the external load to optimize the power output of the cell at any given moment. There are different MPPT techniques that can be used for MFCs, including perturbation and observation (P&O) [31,39,45], incremental conductance (IC) [8], and hill climbing. MPPT can significantly increase the power output and efficiency of MFCs, making them more practical for various applications, including energy production and wastewater treatment. Several custom-designed PMSs with MPPT capabilities have been reported to date. J.D. Park et al. reported a hysteresis controller-based system with digitally controllable potentiometers to continuously track the MPP, achieving 99.2 % energy extraction but only transferring 35.9 % to output capacitors due to losses in the diode of the boost converter [25,39]. To improve efficiency, a synchronous boost converter was used, resulting in an efficiency increase from 43.8 % to 75.9 % [46]. Erbay et al. developed a monolithic PMS with dynamic MPPT using capacitive dividers, achieving 30 % efficiency [44]. Another study by the same research group used a Dickson converter and a time multiplexing approach for harvesting energy from MFC arrays, reporting 65 % efficiency [47]. Alaraj et al. presented a PMS with MPPT and voltage overshoot avoidance using an off-the-shelf boost converter and an extremum seeking approach but the system's efficiency was not reported [48]. Nguyen et al. introduced a parallel-charging, series-discharging PMS achieving 59 % efficiency by estimating MPP from the MFC's open circuit voltage [40].

Moreover, due to their convenient modularization, multiple MFC modules are frequently utilized across various applications. As a result, there is a growing need to develop PMSs capable of simultaneously extracting and harvesting energy from multiple MFCs, each operating at its respective MPP. These PMSs should also be highly efficient in converting the harvested energy into a usable level suitable for powering external devices and electronics. In this study a novel PMS that performs MPP tracking and energy harvesting of up to five MFCs is developed. The PMS keeps the output voltage within a range and allows the connection of external loads such as LEDs or sensors to use the excess energy. Moreover, two different external power backup systems are available within the PMS and can be utilized to complement the energy generated by the MFCs, in instances where the latter proves to be insufficient to power the electronic devices.

2. Materials and methods

2.1. Maximum power transfer theorem and MFC equivalent electrical circuit

The principle of maximum power transfer indicates that the highest power transmission occurs between a power source and a load when their respective impedances are equal. Mathematically, this theorem can be expressed as follows:

$$P_{max} = \frac{V^2}{4R} \tag{1}$$

where P_{max} is the maximum power transfer, V is the voltage of the source, and R is the internal resistance of the source. Fig. 1A shows the conventional equivalent electrical circuit of a MFC [49,50], where V_{MFC} is the MFC's potential, R_{OHM}, R_{ACT}, and R_{CON} represents the ohmic, activation and concentration losses respectively, and C_{DL} represent the double layer capacitance. Nonetheless, it is possible to simplify the equivalent electrical circuit of a MFC (as depicted in Fig. 1B) once it reaches a steady state, at which point the contribution of the double layer capacitance becomes negligible. Under such circumstances, an MFC can be represented by a voltage source connected in series with a resistor, which accounts for the total internal resistance of the cell. This has implications for the implementation of the MPPT algorithm, as will be discussed in 2.3.

2.2. PMS design and operation

Simulations were conducted using MATLAB Simulink to guide the design of a PMS and its operation conditions. Several PMS configurations were studied in the simulations, and the parameters of commercially available integrated circuits were utilized to obtain the most precise outcomes. The main objective of the simulations was to optimize the efficiency of the PMS under various conditions, while concurrently facilitating the design of a Printed Circuit Board (PCB) that could accommodate all the necessary components to control up to five MFCs at their MPP, harvest their energy, regulate the output voltage, and effectively manage the energy to ensure efficient power delivery to the PCB. The simulations facilitated the comparison of multiple MPPT algorithms. Additionally, the simulations were utilized to determine the appropriate sizing of electronic components and operating parameters such as frequency, as well as to test various boost converter configurations, output voltage regulation methods, and different MFC array configurations in order to enhance performance.

Fig. 2 illustrates the PCB final design. Each MFC is connected to the PCB through screw terminals. Individual Boost Converters (BC) are allocated to each MFC to track their MPP. Screw terminals are also present at the output of each BC, enabling the combination of outputs in series and/or parallel, as per requirements. The right-hand side of the PCB is utilized for energy harvesting and voltage regulation. A detailed description of each segment of the PCB is elaborated below.

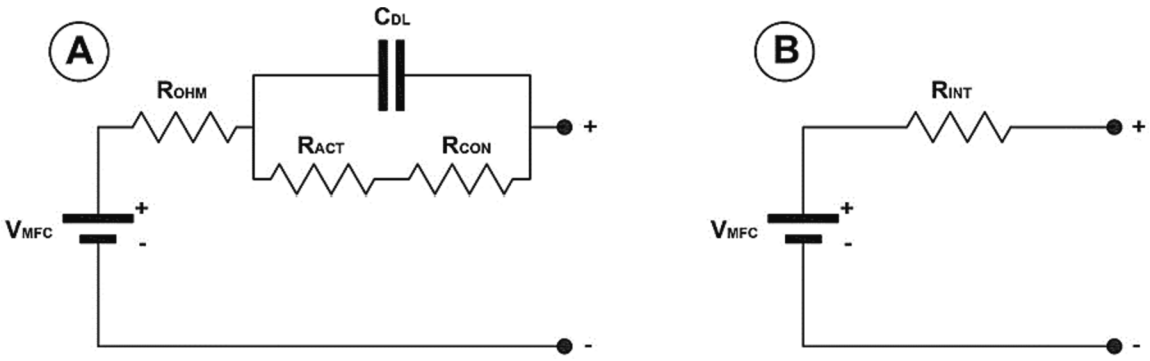

Fig. 1. A) MFC equivalent electrical circuit. B) MFC equivalent electrical circuit under steady state conditions.

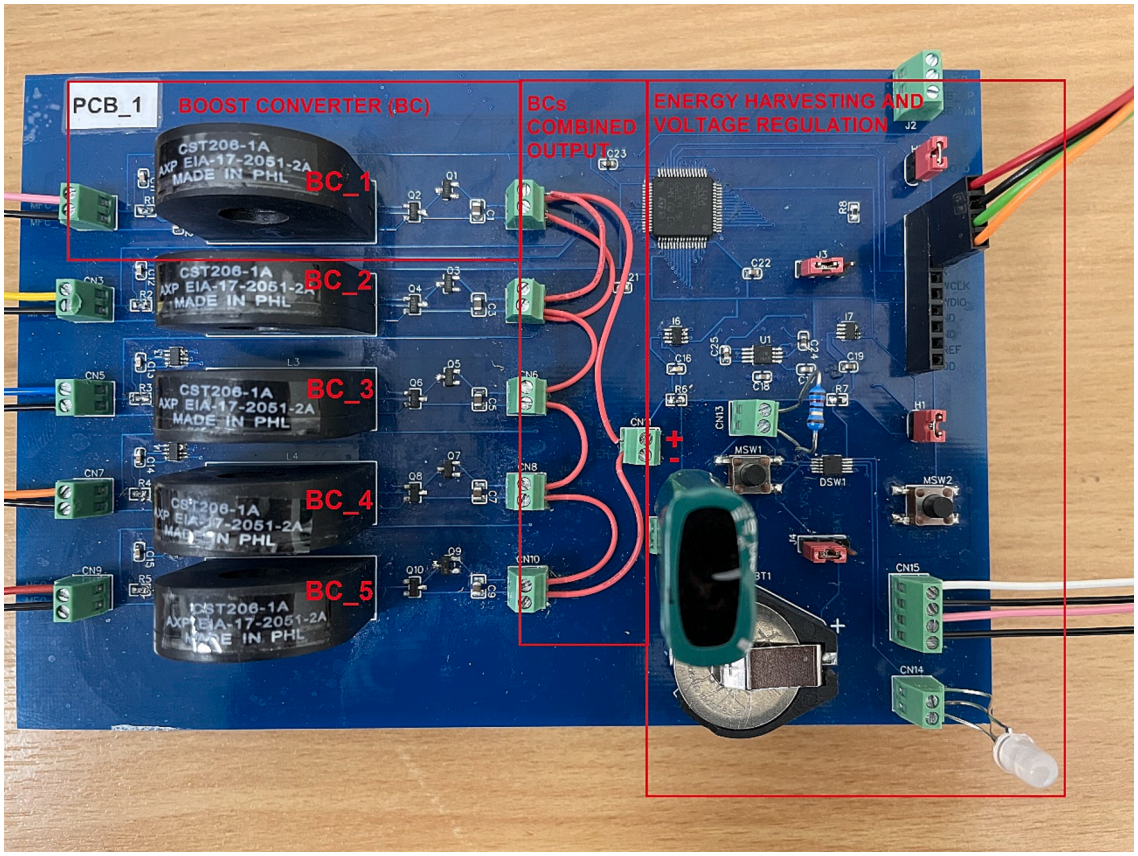

Fig. 2. Picture of the PCB incorporating the PMS with the capacity to perform MPPT for up to five MFCs, as well as energy harvesting, voltage regulation, and power management functions.

2.2.1. Boost converter

BCs possess the capability to alter their input impedance whilst simultaneously elevating the input voltage. The input impedance of a BC can be estimated by utilizing the following approximation.

$$Z_{BC} \approx \frac{2 \times L \times f}{D^2} \quad (2)$$

where Z_{BC} is the BC input impedance, L is the converter's inductor, f is the switching frequency of the MOSFET switch and D is the duty cycle. Consequently, by controlling the duty cycle a BC is able to adjust its internal resistance to that of the MFC, thereby enabling real-time tracking of its MPP while simultaneously elevating the voltage of the MFC.

The schematic diagram of the BC circuit designed in this study is depicted in Fig. 3. All the five BCs are identical. In this study, a synchronous BC configuration was employed. The BC was constructed utilizing a 1 μF input ceramic capacitor (C_{in}), a 14 mH inductor (L, CST206-1A, Triad Magenetics), a N-channel MOSFET (*M1*, DMG3414U-7, Diodes Incorporated), a P-channel MOSFET (*M2*, DMP1045U-7), and a 10 μF output ceramic capacitor, (R_s) and a current sense amplifier.

An ultra-low power microcontroller (STM32L452RE6T, ARM) directly measures the voltage of the MFC. The MFC current is measured by a current sense amplifier (*Isense*, INA190A4IDDFR, Texas Instruments) using a shunt resistor (R_s) which is connected in series with the inductor. To minimize energy losses and increase efficiency, a 1 Ω shunt resistor was selected. The INA190 amplifies the voltage drop across the shunt resistor by 200, and this voltage is measured by the microcontroller (MCU). The MFC's power is determined by the multiplication of its current and voltage.

The MCU employs pulse width modulation (PWM) at a frequency of

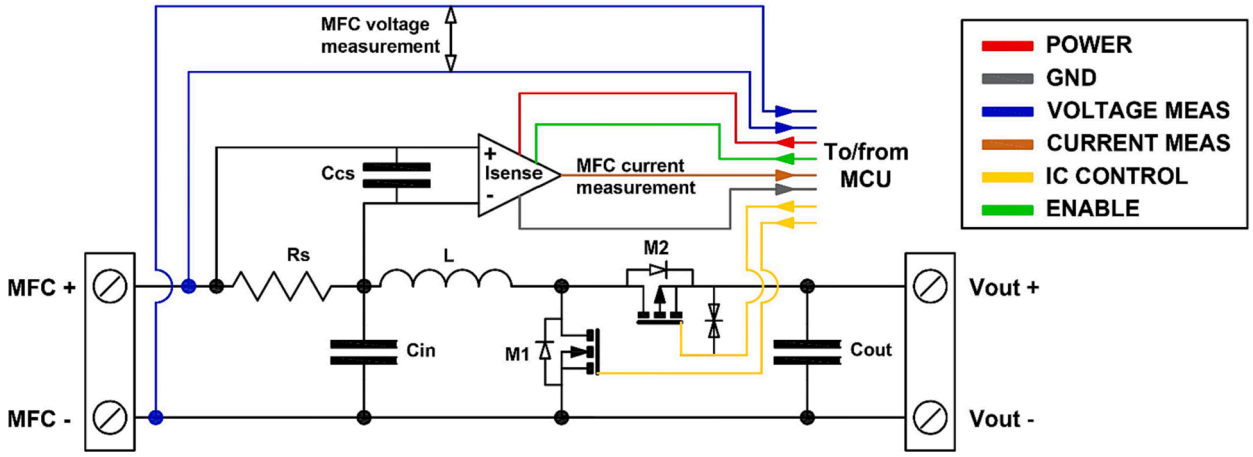

Fig. 3. Schematic diagram of the boost converter circuit.

10 kHz to regulate the N and P-channel MOSFETs. To lower power consumption and enable a duty cycle resolution of 1 μs, the MCU clock frequency was reduced to 1 MHz. This reduction provides the ability to have up to 100 different values for the duty cycle.

2.2.2. *Energy harvesting and voltage regulation*

The schematic diagram of the energy harvesting, and voltage regulation circuit is shown in Fig. 4. A 5F supercapacitor (*SC*) is utilized to store the energy that is harvested from the five MFCs. It is worth noting that the energy produced by the MFCs may exceed or fall short of the required amount to power all the electronics present in the PCB. To regulate the excess energy, a digital dual switch (*DDsw*, TS3A24159, Texas Instruments), controlled by the MCU, is utilized to connect a load, such as a resistor, diode or sensor, when necessary. Additionally, the switch can connect the supercapacitor to a power supply to charge it to a predetermined voltage level. This feature proves particularly valuable in scenarios where the energy output from the MFCs falls short of sustaining the PCB's operation, notably during MFC start-up phases or instances of low COD feeding events. The user can select between two power sources by adjusting the jumper (*J1*) position. The available voltage sources include a 3 V coin cell battery on the PCB or an external voltage source connected to the designated pin on the header. A tactile switch is also included to initiate operation manually in the event that the board voltage falls below 1.71 V, which represents the minimum

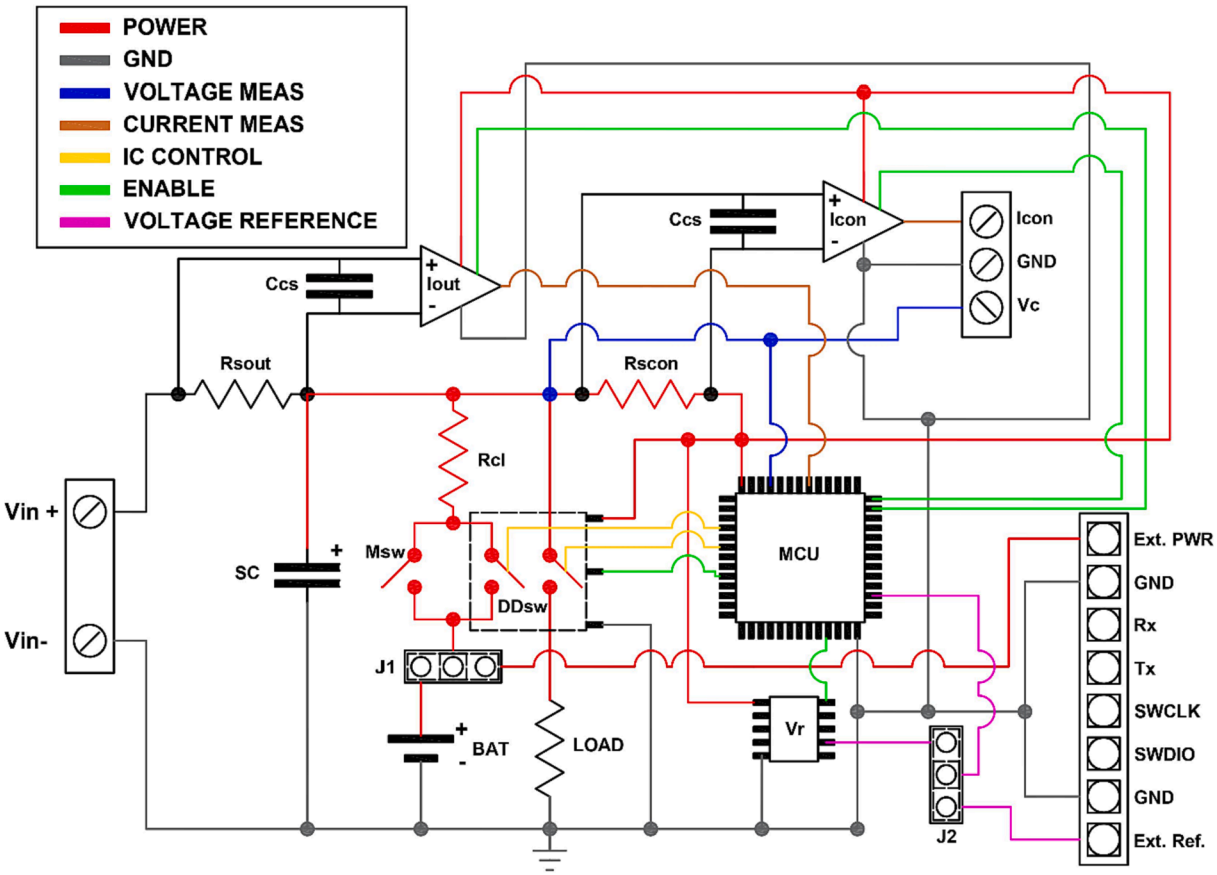

Fig. 4. Schematic diagram of the energy harvesting and voltage regulation circuits.

power voltage required for the MCU to function.

The measurement of output current (I_{out}) flowing from the MFCs to the supercapacitor is conducted by using a current sense amplifier INA190 in conjunction with a 1 Ω shunt resistor (R_{sout}). Meanwhile, the supercapacitor voltage (V_{out}) is directly measured by the MCU. By multiplying both values, the output power (P_{out}) is calculated. The input power (P_{in}) is calculated by summing the individual power of each of the five MFCs as explained in the previous section. The efficiency of the printed PCB is subsequently determined by dividing P_{out} by P_{in}.

To estimate the power consumed by the MCU under different conditions, a data logging system based on virtual instruments (LabVIEW™, National Instruments Inc) was employed. The system was connected to analog inputs on the I/O card (NI-USB-6218) for data acquisition. The data logger was connected to the board via screw terminals in order to measure the voltage of the MCU, as well as the amplified voltage across the 1 Ω shunt resistor (R_{scon}) by a current sense amplifier INA190. This allowed for the calculation of the power consumed by the MCU. It is worth noting that the voltage of the MCU is identical to that of the supercapacitor ($V_{out} \approx V_c$), due to the negligible voltage drop across the shunt resistor.

In this study, a voltage regulation method based on hysteresis was employed with the aim of maintaining the output voltage (V_{out}) within a specific range around the setpoint value. The proposed approach involves alternating prolonged charging and brief discharging periods in instances where there is an excess of energy produced by the MFC, enabling the operation of the connected load. Three voltage values are specified on the MCU script, the desired output voltage (V_D), the lower voltage threshold, (V_{LTH}) and the upper voltage threshold (V_{UTH}). If the output voltage drops below V_{LTH}, the MCU will activate the external power supply, and the supercapacitor will charge until the output voltage reaches V_D. Conversely, if the output voltage exceeds V_{UTH}, the MCU will engage the load, which is an LED in this case, to discharge the supercapacitor until the output voltage reaches V_D.

The integrated circuits mounted on the PCB receive their power supply directly from the supercapacitor. The voltage level of the integrated circuits is the same as the voltage level of the supercapacitor. Therefore, the MCU voltage is continuously changing as a result of the hysteresis-based voltage regulation technique. To ensure a steady voltage reference of 3.3 V for analog measurements, a buck-boost converter voltage regulator (V_r, TPS60240DGKT, Texas Instruments) has been incorporated. Users also have the option of using an external voltage reference by connecting it to the assigned header pin and changing the jumper (J2) accordingly.

2.3. MPPT algorithm

A variable step size incremental conductance (IC) method was employed to determine the MPP of the MFCs. The basic principle of the IC method is to compare the incremental conductance (dI/dV) of the MFC system with the instantaneous conductance value (I/V), which is calculated based on the operating voltage and current of the MFC system. The IC algorithm running on the MCU modifies the duty cycle (D) of the BC to adjust the output voltage of the MFC. The flowchart of the IC algorithm is presented in Fig. 5. ΔD denotes the magnitude of the duty cycle increment or decrement for each iteration. In this study, a variable size ΔD was utilized with the aim of accelerating the rate of convergence, particularly during the initialization stage of the algorithm and in instances of significant fluctuations in power. The calculation of ΔD is expressed as follows:

$$\Delta D = \frac{10 \times (P(t) - P(t-1))}{P(t)} \tag{3}$$

where $P(t)$ represents the power of the MFC in the present iteration, and $P(t\text{-}1)$ represents the power of the MFC in the preceding iteration. In order to prevent unstable behaviour of the IC algorithm resulting from large ΔD values, a restriction was imposed on the maximum allowable value of ΔD. Specifically, this value was capped at 5 % of the duty cycle's full scale. Due to the same rationale, the minimum duty cycle value was established at 5 %, and the maximum at 95 % out of the 100 available values. When the code is initialized, the duty cycle starts at 69 %. Following every modification of the duty cycle, the MFC is allowed to reach equilibrium before its current and voltage are measured. After the completion of this measurement, the MPPT algorithm proceeds with another iteration, and this process is repeated indefinitely. Within the Data Availability section, there is a hyperlink available for accessing the source code of the MCU responsible for managing the PMS and the MPPT implementation.

2.4. MFC construction and operation

Five MFC tubes were assembled, each comprising five MFC modules. These constructions followed the method outlined in [51], utilizing a cation exchange membrane (CMI7000S, Membrane International Inc.,

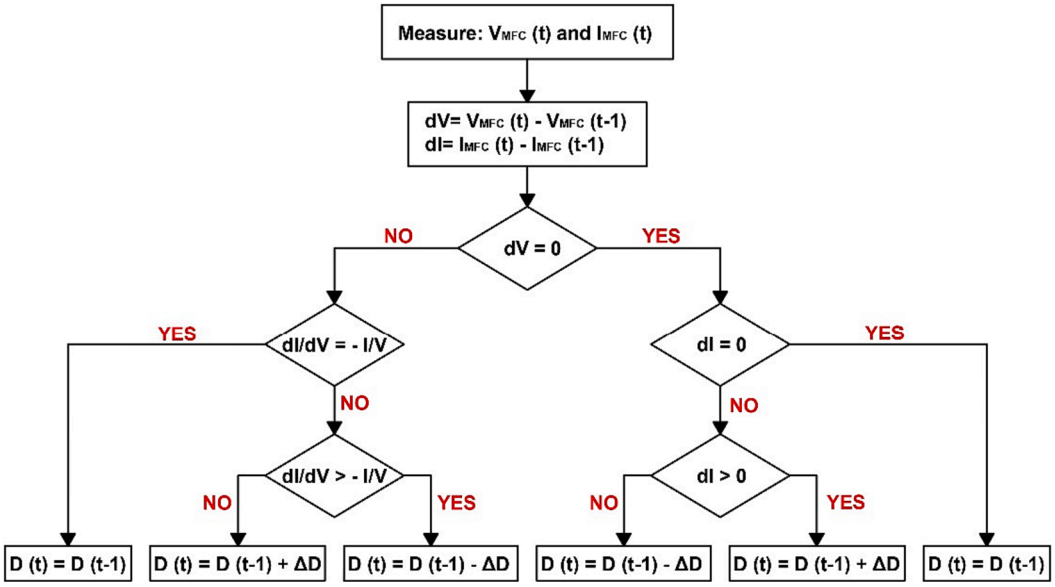

Fig. 5. Flowchart of the incremental conductance algorithm.

NJ, USA). However, instead of using helical anodes, 6 mm rod anodes were utilized. In each of the membrane tubes, five cathodes were installed with a separation distance of 1 cm between them. Coaxially positioned within the tube assembly, five anodes were aligned with their corresponding cathode. To create a larger MFC for the experiments in this study, the cathodes of each tube were connected together, as well as all the anodes of each tube. The MFC tubes had an approximate empty bed volume of 1.6 L each. The five tubes were hydraulically connected in series by utilizing Marprene tubing (Watson Marlow) with an inner diameter of 1/8″. The MFC assembly was supplied with a blend of untreated wastewater collected from the inlet of a wastewater treatment plant (Builth Wales, UK) and synthetic sewage prepared according to the OECD guidelines, which had a Chemical Oxygen Demand (COD) strength of approximately 1000 mg/L. This mixture was fed to the MFC assembly from a reservoir with a capacity of 20 L, in a 1:1 ratio. Polarization curves were conducted utilizing resistance decade boxes (71–7270, Tenma) and a datalogger (NI-USB-6218, National Instruments).

2.5. Experimental design

The experiments were conducted in two distinct configurations. Due to the challenging task of regulating the open circuit potentials and power outputs of five MFCs to assess the performance of the PMS under varying conditions, five autonomous data acquisition devices (NI-USB-6009, National Instruments) and 39 Ω resistors were utilized. These components were employed to mimic the electrical circuitry of the MFCs under steady state operating conditions, as illustrated in Fig. 1B. The simulated MFC's power outputs were altered using the analog output from the data acquisition devices. The theoretical MPP was calculated utilizing equation (1). The aforementioned approach facilitated the examination of the PMS's effectiveness and efficiency under various experimental conditions. The frequency of iteration for the MPPT algorithm was fixed at 5 s. It is worth noting that the internal capacitance of the MFC was disregarded in this experimental setup, making longer waiting periods for the MFC to achieve steady state after each MPPT algorithm iteration unnecessary.

The second experimental configuration entailed the implementation of the PMS on five tubular MFCs connected in series. In this instance, the frequency of iteration for the MPPT algorithm was set at 60 s, allowing the MFC sufficient time to stabilize following each perturbation. This adjustment was necessary as the MFC's internal capacitance must now be considered. Furthermore, since the MFC current was significantly higher than in the first experimental setup, the 1 Ω shunt resistors were replaced with 0.2 Ω shunt resistors to prevent the INA190 current sense amplifiers from saturating. The MFCs were operated in batch mode and fed with the mixture detailed in the preceding section.

3. Results and discussion

3.1. Operation of the N and P-channel MOSFETS

Based on the simulations conducted in MATLAB Simulink, the PMS was developed with the aim of regulating the MPP of each MFC independently. This measure was taken to prevent voltage reversal. Additionally, synchronous BCs were employed, and their output capacitors connected in series to enhance the efficiency of the overall system. However, there are a few technical issues that require to be addressed.

In a synchronous BC, the diode is substituted with a P-channel MOSFET switch to circumvent the issue of high forward voltage drop at the diode. However, MOSFETs have the capability to conduct bidirectional currents. Therefore, a negative inductor current may occur if the P-channel MOSFET is not deactivated when the current reaches a value of zero. This results in the discharge of energy stored in the output capacitor of the BC through the switch and the inductor, back to the MFC. This reverse power flow has the potential to reduce the efficiency of the system. This problem has been addressed in the academic literature by using a zero current switching tracking loop [41] or by implementing a voltage threshold for the P-channel MOSFET [46]. These approaches require additional electronic components and are complex. In this study, an approach that does not require any extra components was used. The MCU controls both the N and P-channel MOSFETS. In the MCU, the specified duty cycle for the N-channel MOSFET governs the duration for which the switch remains closed, while in the case of the P-channel MOSFET, it regulates the duration for which the switch remains open. Consequently, if both MOSFETs have identical duty cycles, when one MOSFET opens, the other MOSFET closes, and vice versa. An investigation was conducted to prevent the occurrence of negative currents flowing back into the MFC by introducing a delay between the opening of the N-channel MOSFET and the closing of the P-channel MOSFET. This delay results in a decrease in the amount of time that the P-channel MOSFET remains closed, thereby reducing the likelihood of encountering the negative current problem. The duty cycle of P-channel MOSFET can be written as follows:

$$D_{P-CH} = D_{N-CH} + d \tag{4}$$

where $D_{P\text{-}CH}$ and $D_{N\text{-}CH}$ denote the duty cycles of the P-channel and N-channel MOSFETs, respectively, while d represents the delay as a fraction of the full-scale duty cycle. In order to assess the impact of distinct d values on the power output extracted from the electrically analogous MFCs while maintaining consistent operational parameters, all five BCs were subjected to a diverse range of duty cycles. The outcomes of this experiment are depicted in Fig. 6. The findings exhibit a power curve-like pattern. This is because the impedance of the BC, as well as its ability to extract power from the MFCs, change with variations in the duty cycles. It should be noted that the operating parameters of the MFCs remained constant throughout the experimentation. The most efficient method of operating both MOSFETs was found to be with no delay (d = 0) between them, provided that the duty cycles were above 0.3. At lower values of duty cycles, increasing the delay was found to be more beneficial. This can be attributed to the fact that as the duty cycle decreases, the N-channel MOSFET spends less time in the closed state, resulting in less energy being stored in the inductor. Conversely, the P-channel MOSFET remains closed for longer periods, discharging the energy stored in the inductor and increasing the likelihood of current reversing from the output capacitor to the MFC. When duty cycles exceed 0.3, a reduction in power extraction occurs as the delay between MOSFETs increases. This is due to the P-channel MOSFET remaining

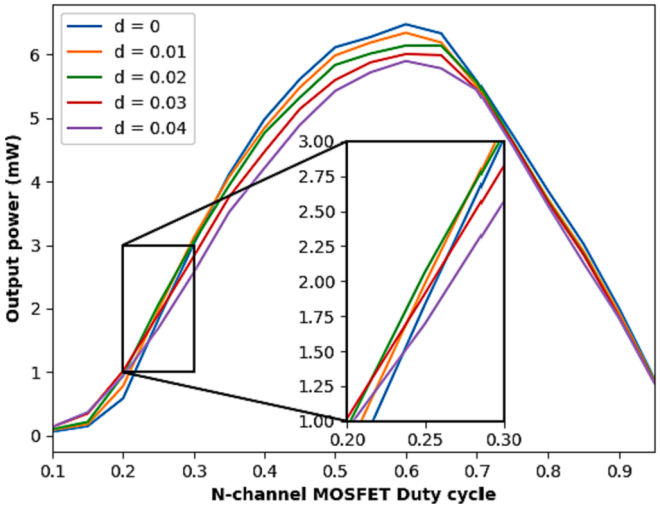

Fig. 6. Output power response of the power management system at varying duty cycles of N-channel MOSFET and delays (d) between the N and P-channel MOSFETs.

closed for a shorter period of time, which does not allow sufficient time for the energy stored in the inductor to discharge. During the course of this investigation, it was observed that the duty cycles of all 5 BCs remained consistently above 0.5, even in situations of extreme conditions. Therefore, no additional delay was implemented between the MOSFETs in the subsequent experiments.

The duty cycle of P-channel MOSFET can be calculated using equation (4). Experimental conditions: The experiment was conducted with the MFC_{OCP} set to 0.5 V for the five MFCs, and the equivalent internal resistance set to 39 Ω. The output voltage of the PCB was fixed at 3.3 V, and all output capacitors of the boost converters were connected in series, except for the top two boost converters that were connected in parallel with each other and in series with the remaining boost converters (Fig. 2).

The voltage output of a MFC is typically low, and achieving the desired output voltage level would require a high duty cycle, which would lead to high energy losses. However, if the output capacitors of each MFC BC are connected in series, the voltage step-up requirement of each BC would be significantly reduced. For example, if five BCs, each extracting the energy from five identical MFCs, were connected in series to attain a 3.3 V output voltage, ideally, each BC would only need to amplify the MFC voltage to 0.66 V (3.3 V / 5), and this would be the voltage across the output capacitor of each BC. As a result, there would be a substantial reduction in the boosting ratio, lowering the duty cycle, thereby enhancing efficiency.

In this case, an additional factor that should be considered is the gate-source threshold voltage ($V_{GS(TH)}$) of the MOSFETs, which denotes the voltage requisite to activate the MOSFET as the gate-source potential differential. In this study, both the N and P channel MOSFETs were selected to have the lowest $V_{GS(TH)}$ as possible, being the typical $V_{GS(TH)}$ of the N and P channel MOSFETs 0.7 and −0.55 V respectively. In the instance of the N-channel MOSFET, the gate-to-source voltage (V_{GS}) is calculated by deducting the source voltage, which refers to the voltage of the negative terminal of the output capacitor of the corresponding BC, from the operating voltage of the MCU. In the case of the P-channel MOSFET, the calculation of V_{GS} involves the subtraction of the voltage at the positive terminal of the output capacitor of the determined BC from the voltage at the ground terminal of the MCU, which is set at 0 V in this instance. Therefore, if all the five output capacitors of the five BCs are connected in series, the MOSFETs operated at lowest V_{GS} would be the P-channel MOSFET of BC_5 and the N-channel MOSFET of BC_1 (refer to Fig. 2). The gate voltage of the P-channel MOSFET of BC_5 is at 0 V, and the source voltage in this scenario corresponds to the voltage across the output capacitor of BC_5. In the ideal scenario previously mentioned, the V_{GS} would be −0.66 V, which would suffice to activate the P-channel MOSFET. Even if the V_{GS} voltage does not reach the $V_{GS(TH)}$, current would still flow through the MOSFET's diode (See in Fig. 3), although at the expense of a significant forward voltage drop at the diode. The N-channel MOSFET of BC_1 has a gate voltage equivalent to the operating voltage of the MCU. In this situation, the source voltage corresponds to the voltage of the negative terminal of the output capacitor of BC_1. Referring to the ideal example stated earlier, the V_{GS} of the P-channel MOSFET can be calculated as 3.3 – 3.3 x 4 / 5 = 0.66 V. Consequently, the N-channel MOSFET would not be activated, resulting in a malfunctioning BC_1. It is important to note that in case the target output voltage is less than 3.3 V, the V_{GS} of the P-channel MOSFET of BC_1 would be further reduced. For the current research, the output voltage was modified within the range of 2.4 to 3.3 V, which is consistent with the logic HIGH output range of a 3.3 V CMOS device. As a result, the in-series connection of all output capacitors of the BCs has been excluded. Instead, two distinct connection combinations have been examined. The first combination involves connecting the output capacitors of BC_1 and BC_2 in parallel and then in series with the output capacitors of BC_3, BC_4, and BC_5 (1//2–3–4–5), as illustrated in Fig. 2. The second combination entails connecting the output capacitors of BC_1 and BC_2 in parallel and then in series with BC_3, and the resulting in parallel connection between BC_4 and BC_5 (1//2–3–4//5). The rationale underlying these two combination alternatives is to elevate the voltage across the output capacitors, particularly at BC_1, in order to guarantee its proper functioning. An alternative approach would be to connect all the output capacitors of the BCs in series to charge the supercapacitor at a lower voltage level, such as 1.8–2.4 V. Subsequently, the buck-boost converter voltage regulator utilized to provide a reference to the MCU (refer to section 2.2.2) can be positioned after the supercapacitor to amplify the voltage further to 3.3 V. This arrangement offers the benefit of enabling the N-channel MOSFET of BC_1 to function correctly in any situation, facilitating the in-series connection of the five BCs and presumably enhancing their efficiency. However, to determine the overall system efficiency, one would need to multiply the efficiency of the first boosting stage - derived from the combination of the MFC boost converters to reach 1.8–2.4 V - by the efficiency of the buck-boost converter voltage regulator. The efficiency of the latter would be approximately 0.83, considering an input voltage of 2.4 and an output current of 10 mA. Therefore, the overall PMS efficiency would likely be less than 0.8.

3.2. Efficiency and power consumption of the PMS

The objective of this section was to assess the influence of two distinct configurations for connecting the output capacitors of the BCs that were discussed in the preceding section. This was accomplished by measuring the efficiency of the PMS over a broad range of desired output voltage levels and MFC open circuit potentials. The results are presented in Fig. 7. As anticipated, the efficiency of the PMS reduces as the output voltage increases and as the open circuit potentials of the MFCs decrease. In both scenarios, the lower efficiency is due to the need for higher boosting ratios at the BCs. The efficiency of the PMS experiences a sharp decline when there is a combination of higher output voltage and lower MFC open circuit potentials. In reality, the OCP of the MFCs is a fixed parameter, however, it varies depending on the specific application. Nevertheless, this data emphasizes the significance of the MFC operating conditions in determining the overall efficiency of the PMS, since the desired output voltage is typically fixed. This contrasts with most PMSs described in the literature, which usually report a single efficiency value. At an output voltage level of 2.4 V, in most real-world applications, the PMS is typically expected to achieve efficiency levels ranging between 0.85 and 0.87 and 0.55–0.73, when the individual BCs are connected in the 1//2–3–4–5 and 1//2–3–4//5 configurations, respectively. However, if the desired voltage output is increased to 3.3 V, the efficiency levels of the PMS are likely to fall within the range of 0.81–0.63 for the 1//2–3–4–5 connection, and between 0.54 and 0.25 in the case of the 1//2–3–4//5 connection. It is evident that the 1//2–3–4–5 connection configuration exhibits significantly higher efficiency values as compared to the 1//2–3–4//5 configuration. This is attributed to the lower boosting ratio requirement at each boost converter. As a result, further testing was conducted on the 1//2–3–4–5 connection configuration in subsequent experiments. The authors believe, that relocating the buck-boost converter voltage regulator in order to increment the MFC voltages in two stages, as discussed in the preceding section, is unlikely to enhance the efficiency of the system. This is particularly true in cases where the open circuit potentials of the MFCs exceed 400 mV, given that the efficacy in the presented configuration already exceeds 0.75.

When selecting the desired output voltage of the PMS, it is important to consider power consumption, particularly if the PCB is intended to be powered exclusively with the energy harvested from the connected MFCs. Each current sense amplifier and buck-boost converter voltage regulator draw a current of 65 μA and 250 μA, respectively, when enabled, and only 0.1 μA when disabled. To minimize power consumption, these components are activated solely during the measurement of current and voltage values, which typically lasts for a few milliseconds. Therefore, they are kept disabled during most of the operating time. The PCB has a power consumption of 3.2 mW when

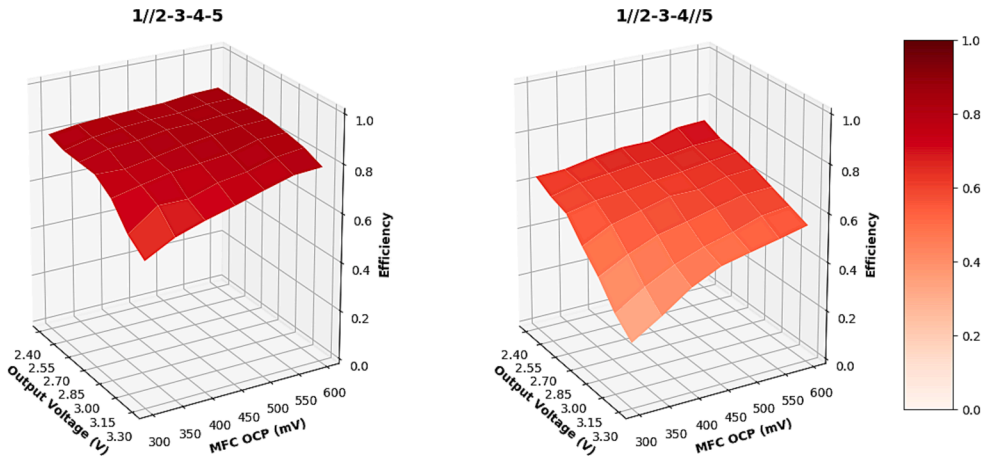

Fig. 7. PMS efficiency at different output voltages and MFC open circuit potentials when the output capacitors of the boost converters are connected in the 1//2–3–4–5 and 1//2–3–4//5 configurations respectively.

operating at 2.4 V, and this power consumption exhibits a linear increase with a slope of 2.87 mW/V. As a result, the power consumption at a voltage of 3.3 V can be calculated as 3.2 + (3.3–2.4) x 2.87 = 5.78 mW.

3.3. Maximum power point tracking testing

In order to evaluate the PMS's capacity to monitor the MPP of five MFCs concurrently, simulated MFCs were subjected to sudden changes in power. The theoretical MPP was determined using equation (1). The experimental protocol involved modifying the maximum power output of the MFCs in the range of 0.25 to 2.5 mW. Specifically, odd-numbered MFCs were manipulated to vary from high to low power, while even-numbered MFCs were adjusted from low to high power. The rationale for the adoption of this experimental configuration was to evaluate the efficacy and response time of the PMS to track the MPP across a diverse range of MFC power outputs. The experimental setup accounted for situations in which the power outputs of the individual MFCs exhibited significant differences as well as those in which the power outputs were comparable. Of particular interest was the impact of this broad range of scenarios on the output voltage (*BCvout)* and Duty cycles of each individual boost converter. The results are shown in Fig. 8.

The observations from Fig. 8 reveal that the MPPT algorithm can closely track the MPP of all five MFCs simultaneously. Although minor deviations from the MPP can be observed after each perturbation, the variable step size Incremental Conductance MPPT algorithm can identify the new MPP within a few iterations. Subsequent to each perturbation, the MPPT algorithm applies higher ΔD values in accordance with equation (3). Once the MPP is reached, the duty cycle oscillates between values that result in the power output closest to the MPP. At low MFC power outputs, the duty cycle appears more erratic since there may be more variance in power calculations, and thus in the calculation of ΔD, but does not affect the tracking of the MPP. Nevertheless, since the power output of MFCs changes gradually, significant deviations from the MPP are not expected to occur in practice.

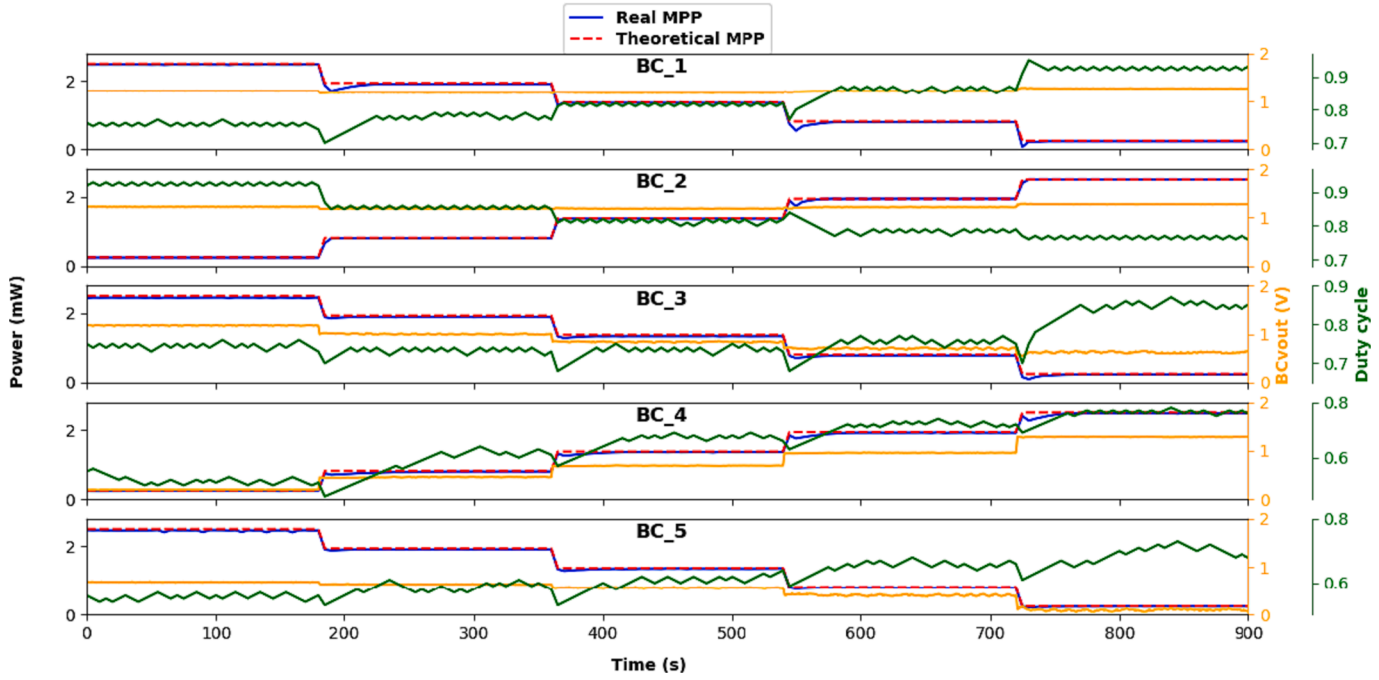

Fig. 8. PMS response to simulated MFC power perturbations and effect on the output voltage and duty cycle of each individual boost converter. Experimental conditions: Boost converters connected in the 1//2–3–4–5 configuration and PMS voltage output set to 3.3 V.

An observation to note from Fig. 8 is that the output voltage of the boost converters belonging to MFC_1 and MFC_2, which are connected in parallel, remained above 1.1 V even when the output power of the MFCs was only 10 % of the other one. Furthermore, the output voltage of these boost converters, when connected in parallel, was significantly higher than the rest. Thus, connecting the boost converters of MFC_1 and MFC_2 in parallel effectively generated a sufficiently high output voltage to ensure proper functioning of the N-channel MOSFETs, even when MFC_1 or MFC_2 had very low output voltages. However, the output voltage of the boost converter of MFC_5 varied between 0.1 and 0.7 V, suggesting that the P-channel MOSFET of this boost converter might not have been closing at some power levels, especially at low MFC power outputs. Nevertheless, this does not affect the MPPT of this particular MFC since, as mentioned earlier, current can still flow through the external MOSFET's diode, although it decreases the efficiency of the PMS.

Kim et al. [16] employed two commercially available boost converter and power management chips (LTC3108, Analog Devices) to extract the energy and step up the voltage of two MFC. The configuration was such that each MFC provided power to its corresponding LTC3108 chip which output was used to charge an output capacitor at a voltage of 3.3 V. A few hours after connecting in series the outputs of the aforementioned capacitors with the intention of boosting the output voltage, and the discontinuation of the feed supply of one of the MFCs (MFC_1), a voltage reversal was detected in one of the capacitors. The authors postulated that this could be attributable to kinetic imbalances between the two capacitors connected in series, stemming from the insufficient energy of MFC_1 to maintain the voltage output of PMS_1. However, the current study did not observe this phenomenon. Despite the MFC's output power being a fraction of the output power of the preceding and subsequent MFCs, whose output capacitors are connected in series, such as in the case of MFC_4 at the start of the experiment depicted in Fig. 8, voltage reversal does not occur. It is worth noting that, even in this scenario, the output voltage remained above 0.1 V, making a small but positive significant contribution to the overall voltage output, despite the low power output of the MFC. In this particular PMS design, the occurrence of voltage reversal in the BC output capacitors connected in series is prevented. This is because the individual BC of each MFC is not constrained to maintain a specific voltage output, which could potentially exceed the MFC's capacity. As illustrated in Fig. 8, the voltage output of each BC is dependent on the power output of the MFC they control, as well as the interconnection of the BC outputs. These BCs function cooperatively to achieve and maintain a voltage output of 3.3 V.

3.4. Application of the PMS to tubular microbial fuel cells connected in series

The designed PMS was employed in the operation of five tubular MFCs connected hydraulically in series. In this case, it is important to consider the internal capacitance of the MFC and introduce a longer delay before re-evaluating the power output of each MFC after adjusting the duty cycle. To verify that the five tubular MFCs were functioning at their MPP, polarization curves were conducted on four separate occasions. To conduct these tests, the MFCs were disconnected from the Printed PCB during the experiments, and subsequently reconnected thereafter. Upon reconnection, the algorithm was restarted, and the MPP algorithm initiated the search for the MPP of each MFC once again. From Fig. 9 it can be observed that the highest power output for each MFC, as calculated from the polarization curves, aligns with the maximum power obtained from each MFC through the PMS at the four different instances. Furthermore, after the reactivation of the variable step size IC algorithm, the power harvested from the MFCs swiftly returns to its previous levels. This implies that a 60-second delay between power measurements is sufficient. Highlighting the significance of the time delay between measurements, it is worth mentioning the ultra-low power boost converter with MPPT capabilities chip (BQ25504, Texas Instruments). To achieve operation at the MPP, the BQ25504 chip periodically opens the circuit every 16 s for a duration of 256 ms to measure the open circuit potential of the source. Then, it regulates the input voltage of the boost converter to be half of the measured open circuit potential to match the source's impedance, thereby ensuring

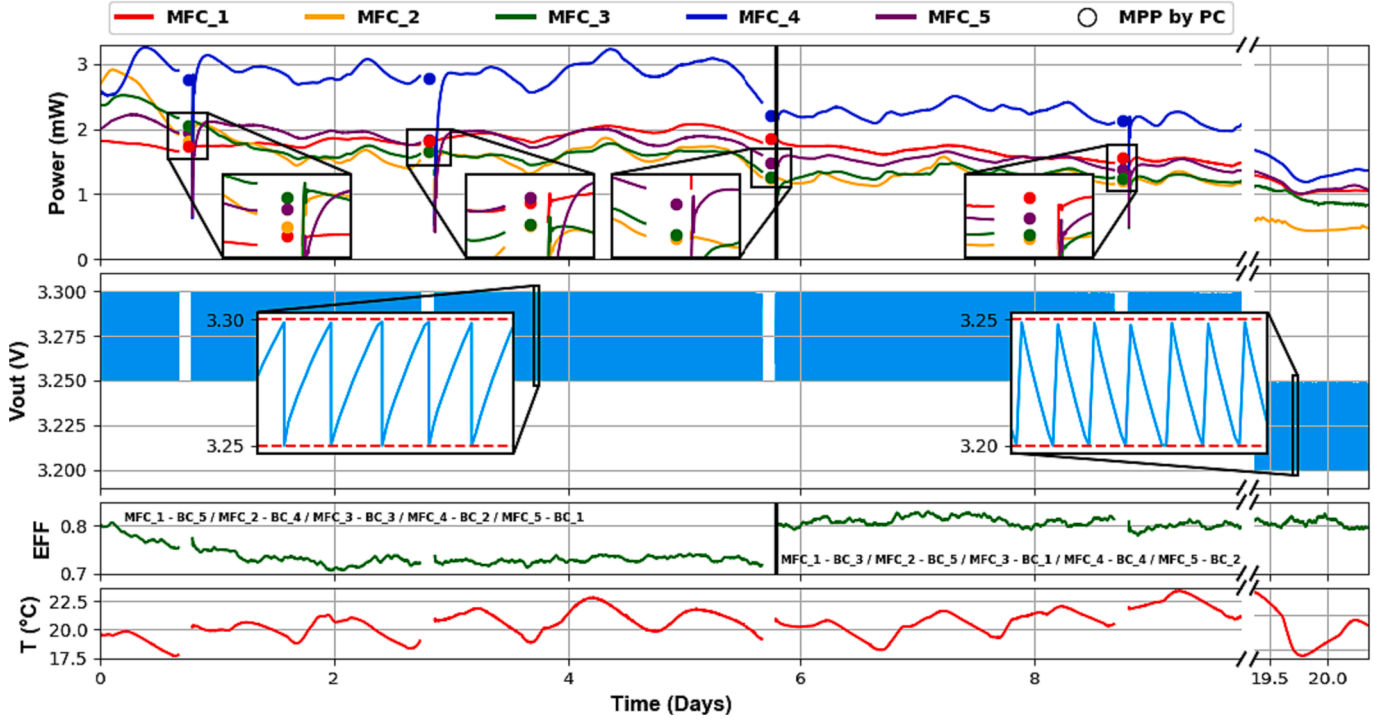

Fig. 9. Power output of each tubular MFC obtained through the PMS, along with the MPP determined through polarization curve analysis, output voltage and efficiency of the PMS, and ambient temperature recorded during the experimental period.

operation at MPP. However, this feature is not practical for tracking the MPP of MFCs since it takes several seconds to reach the open circuit potential, as opposed to a few milliseconds. Consequently, MFCs may operate far from the MPP if this feature is used [34].

Fig. 9 also illustrates the efficiency of the PMS throughout this experiment. Each MFC can be linked to a dedicated BC on the PCB in any sequence. Initially, during the first 140 h of the experiment, MFC_1, MFC_2, MFC_3, MFC_4, and MFC_5 were connected to BC_5, BC_4, BC_3, BC_2, and BC_1, respectively, resulting in an average efficiency of 0.734. Following the third polarization curve, the MFCs were rearranged and connected in the order of MFC_1, MFC_2, MFC_3, MFC_4, and MFC_5 to BC_3, BC_5, BC_1, BC_4, and BC_2, respectively, resulting in an average efficiency of 0.808. During the initial phase of the experiment, the highest performing MFC, MFC_4, was connected to BC_2, which had its output connected in parallel to BC_1, to which MFC_5 was connected. Consequently, this arrangement led to high duty cycles in BC_1 and BC_2, resulting in increased energy losses. However, by connecting the best performing MFCs to BC_3 and BC_4, as done in the second phase of the experiment, a significant boost in the efficiency of the PMS can be achieved. Indeed, in future design iterations, it is possible to incorporate multiplexers onto the PCB for the purpose of efficiently combining the outputs of the BCs in an automated manner. This can be accomplished by implementing a programmed set of instructions within the MCU to govern the multiplexers, enabling them to connect the outputs of each BC in the optimal sequence to maximize efficiency.

One important factor to considered when utilizing this PMS in hydraulically connected MFCs is that, as result of connecting the boost converters in series to boost the output voltage, the anodes of the MFCs are at different voltage levels. Consequently, there exists the potential for current leakage from one anode to another due to their electrical connection through the resistance of the solution. The magnitude of such current is directly dependent on the length of the tubing connecting each MFC, and inversely proportional to the cross-sectional area of the tubing as well as the conductivity of the solution. In this case, 1/8″ I.D. tubing, 1.5 m long was used to connect each MFC in series with the preceding one, and the calculated resistance between anodes was ≈ 1.9 MΩ. Consequently, the resultant leakage current was considered insignificant and did not impact the efficiency of the PMS. However, if the resistance between the anodes were to drop below a few kΩ, there would be an adverse effect on the PMS efficiency, with a significant amount of energy being dissipated in the liquid solution. To prevent this, a flyback boost converter configuration in which the inductor is substituted with a transformer could be utilized instead. The transformer would isolate the MFCs from the boost converter's higher voltage outputs. It is important to note, however, that the transformer's DC resistance should be considered since it may be high, thereby nullifying the benefits of isolating the MFCs to prevent current leakage into the solution.

Finally, as depicted in Fig. 9, the power output of each individual MFC fluctuates throughout the day in response to temperature variations. Moreover, over time, the power gradually decreases as the feed supply is depleted. To evaluate voltage regulation, specific thresholds were established for V_{LTH} (Voltage Lower Threshold) and V_{UTH} (Voltage Upper Threshold). V_{LTH} was determined as 50 mV below the voltage reference V_D, while V_{UTH} was set at 50 mV above V_D. V_D was fixed at 3.25 V due to the limited capability of the MCU to measure voltages exceeding 3.3 V. This limitation arises from the fact that 3.3 V serves as the reference voltage supplied to the MCU for conducting analog readings.

During the majority of the experiment, the MFCs provided an excess amount of energy compared to the requirement for operating the entire PCB. Once the output voltage reached 3.3 V, the surplus energy was utilized to illuminate an LED until the voltage output was reduced to 3.25 V. For instance, when the power output from the 5 MFCs and system efficiency are respectively 10 mW and 0.8, the process of charging the output supercapacitor from 3.25 V to 3.3 V takes approximately 410 s. The LED, along with the in-series resistance, consumes 66 mW. Consequently, once the LED is activated to utilize excess energy, it remains lit for approximately 14 s. In scenarios where a lengthier or more frequent activation of the LED or other loads is necessary, strategic supplementation of energy from an external power supply can be employed. The experiment was conducted until the power provided by the MFCs was insufficient to energize the entire PCB, in order to demonstrate the behaviour of voltage regulation in such circumstances. As the MFCs' output power decreased due to the depletion of the feed, the MCU connected one of the external power sources to supplement the energy obtained from the MFCs. To be more specific, the external load was connected when the output voltage fell below 3.2 V and remained connected until the voltage across the output capacitor reached 3.25 V.

4. Conclusions

A comprehensive PMS has been introduced, designed to effectively track the MPP and harness energy from up to five MFCs. The energy obtained from these MFCs is utilized to provide power to the entire PCB, with any excess energy being directed towards illuminating an LED. In situations where the power derived from the MFCs proves inadequate, an external or onboard power source can be employed to supplement the energy supplied by the MFCs. The tracking of the MPP of each MFC is accomplished through the utilization of a variable step size incremental conductance algorithm. This algorithm effectively regulates the duty cycles of each individual boost converter while simultaneously safeguarding against voltage reversal of the weakest MFC. Synchronous boost converters, wherein the diodes are substituted with P-channel MOSFETs, have been employed to enhance the efficiency of the circuit board. The inclusion of additional electronic components is unnecessary to prevent the occurrence of negative currents flowing back to the MFC through the P-channel MOSFET, as long as a delay is introduced between the deactivation of the N-channel and the activation of the P-channel MOSFETs when operating at duty cycles below 0.3. The PMS efficiency depends upon the desired output voltage and the power output characteristics of the MFCs. By combining the outputs of each MFC boost converter, efficiencies of up to 87 % can be achieved. The voltage from the MFCs can be amplified up to 3.3 V and this voltage is regulated by a hysteresis-based control approach. The current sense amplifiers and voltage regulator buck-boost converter are disabled when not used to save energy. The power consumption of the PCB increases proportionally with the target output voltage, the power consumed at 3.3 V was 5.78 mW. The variable step size incremental conductance algorithm showed the capability to rapidly locate and track the MPP of each MFC. A delay period of 60 s between power measurements was found to allow the tubular MFCs to stabilize following each iteration of the duty cycle change. By strategically connecting the best performing MFCs to BC_3 and BC_4, the efficiency of the PMS can be further enhanced. This study make a significant contribution to the field of MFC energy harvesting and control through its comprehensive solution and valuable guidelines to enhance the PMS efficiency when applied to multiple MFCs. The introduced PMS provides distinct advantages compared to previously reported systems such as individual and rapid MPPT for up to 5 MFCs with energy harvesting capabilities, high efficiency, self-sustaining operation when MFCs provide sufficient energy, backup power sources to ensure uninterrupted operation in all scenarios, and a compact PCB design housing all necessary components for seamless functionality. Furthermore, the study proposes various design modifications and potential features for future implementations, providing valuable insights for other researchers in developing their own PMSs tailored to their specific applications.

Declaration of Competing Interest

The authors declare that they have no known competing financial interests or personal relationships that could have appeared to influence the work reported in this paper.

Data availability

Data will be made available on request.

Acknowledgments

RD and RFF are supported by Royal Academy of Engineering Professor of Emerging Technology Grant: Bio-Electrochemical Processes for Carbon Reduction and Resource Recovery: E-Hance (CiET1819\2\86).

References

[1] A. Nawaz, et al., Microbial fuel cells: Insight into simultaneous wastewater treatment and bioelectricity generation, Process Saf. Environ. Prot. 161 (2022) 357–373, https://doi.org/10.1016/j.psep.2022.03.039.
[2] S. Malik, et al., A perspective review on microbial fuel cells in treatment and product recovery from wastewater, Water 15 (2) (2023) pp, https://doi.org/10.3390/w15020316.
[3] Y. Cui, B. Lai, X. Tang, Microbial Fuel Cell-Based Biosensors, Biosensors 9 (3) (Jul. 2019), https://doi.org/10.3390/bios9030092.
[4] C. Donovan, A. Dewan, D. Heo, H. Beyenal, Batteryless, wireless sensor powered by a sediment microbial fuel cell, Environ. Sci. Technol. 42 (22) (Nov. 2008) 8591–8596, https://doi.org/10.1021/es801763g.
[5] H. Yazdi, L. Alzate-Gaviria, Z.J. Ren, Pluggable microbial fuel cell stacks for septic wastewater treatment and electricity production, Bioresour. Technol. 180 (2015) 258–263, https://doi.org/10.1016/j.biortech.2014.12.100.
[6] H. Liu, R. Ramnarayanan, B.E. Logan, Production of electricity during wastewater treatment using a single chamber microbial fuel cell, Environ. Sci. Technol. 38 (7) (Apr. 2004) 2281–2285, https://doi.org/10.1021/es034923g.
[7] P. Kuntke, et al., Ammonium recovery and energy production from urine by a microbial fuel cell, Water Res. 46 (8) (2012) 2627–2636, https://doi.org/10.1016/j.watres.2012.02.025.
[8] Y.E. Song, et al., Maximum power point tracking to increase the power production and treatment efficiency of a continuously operated flat-plate microbial fuel cell, Energy Technol. 4 (11) (2016) 1427–1434, https://doi.org/10.1002/ente.201600191.
[9] Z. Ren, H. Yan, W. Wang, M.M. Mench, J.M. Regan, Characterization of microbial fuel cells at microbially and electrochemically meaningful time scales, Environ. Sci. Technol. 45 (6) (2011) 2435–2441, https://doi.org/10.1021/es103115a.
[10] R.P. Pinto, B. Srinivasan, S.R. Guiot, B. Tartakousky, The effect of real-time external resistance optimization on microbial fuel cell performance, WATER Res. 45 (4) (2011) 1571–1578, https://doi.org/10.1016/j.watres.2010.11.033.
[11] H.C. Boghani, et al., Controlling for peak power extraction from microbial fuel cells can increase stack voltage and avoid cell reversal, J. Power Sources 269 (2014) 363–369, https://doi.org/10.1016/j.jpowsour.2014.06.059.
[12] L. Zhuang, Y. Zheng, S. Zhou, Y. Yuan, H. Yuan, Y. Chen, Scalable microbial fuel cell (MFC) stack for continuous real wastewater treatment, Bioresour. Technol. 106 (2012) 82–88, https://doi.org/10.1016/j.biortech.2011.11.019.
[13] S. Li, G. Chen, Effects of evolving quality of landfill leachate on microbial fuel cell performance, Waste Manag. Res. 36 (1) (2018) 59–67, https://doi.org/10.1177/0734242X17739969.
[14] S.-E. Oh, B.E. Logan, Voltage reversal during microbial fuel cell stack operation, J. Power Sources 167 (1) (2007) 11–17, https://doi.org/10.1016/j.jpowsour.2007.02.016.
[15] F. Khaled, O. Ondel, B. Allard, and N. Degrenne, 'Voltage balancing circuit for energy harvesting from a stack of serially-connected microbial fuel cells', in 2013 IEEE ECCE ASIA DOWNUNDER (ECCE ASIA), IEEE; IEEE Power Elect Soc; CES; KIPE; IEEJ, 2013, pp. 392–397.
[16] T. Kim, et al., Boosting voltage without electrochemical degradation using energy-harvesting circuits and power management system-coupled multiple microbial fuel cells, J. Power Sources 410 (2019) 171–178, https://doi.org/10.1016/j.jpowsour.2018.11.010.
[17] Y. E. Song, M. M. El-Dalatony, C. Kim, M. B. Kurade, B.-H. Jeon, and J. R. Kim, 'Harvest of electrical energy from fermented microalgal residue using a microbial fuel cell', Int. J. Hydrog. Energy, vol. 44, no. 4, SI, pp. 2372–2379, Jan. 2019, doi: 10.1016/j.ijhydene.2018.08.151.
[18] F.L. Lobo, X. Wang, Z.J. Ren, Energy harvesting influences electrochemical performance of microbial fuel cells, J. Power Sources 356 (2017) 356–364, https://doi.org/10.1016/j.jpowsour.2017.03.067.
[19] A. Mukherjee, et al., Effective power management system in stacked microbial fuel cells for onsite applications, J. Power Sources 517 (2022), 230684, https://doi.org/10.1016/j.jpowsour.2021.230684.
[20] R. Alipanahi, M. Rahimnejad, G. Najafpour, Improvement of sediment microbial fuel cell performances by design and application of power management systems, Int. J. Hydrog. Energy 44 (31) (2019) 16965–16975, https://doi.org/10.1016/j.ijhydene.2019.04.162.
[21] J. Prasad, R.K. Tripathi, Scale-up and control the voltage of sediment microbial fuel cell for charging a cell phone, Biosens. Bioelectron. 172 (2021), 112767, https://doi.org/10.1016/j.bios.2020.112767.
[22] A. Dutta, et al., A review on power management systems: An electronic tool to enable microbial fuel cells for powering range of electronic appliances, J. Power Sources 517 (2022), 230688, https://doi.org/10.1016/j.jpowsour.2021.230688.
[23] I. A. Ieropoulos, J. Greenman, C. Melhuish, and I. Horsfield, 'Microbial fuel cells for robotics: energy autonomy through artificial symbiosis', CHEMSUSCHEM, vol. 5, no. 6, SI, pp. 1020–1026, Jun. 2012, doi: 10.1002/cssc.201200283.
[24] A. Dewan, H. Beyenal, Z. Lewandowski, Intermittent energy harvesting improves the performance of microbial fuel cells, Environ. Sci. Technol. 43 (12) (2009) 4600–4605, https://doi.org/10.1021/es8037092.
[25] H. Wang, J.-D. Park, Z. Ren, Active energy harvesting from microbial fuel cells at the maximum power point without using resistors, Environ. Sci. Technol. 46 (9) (2012) 5247–5252, https://doi.org/10.1021/es300313d.
[26] C. Forrestal, Z. Stoll, P. Xu, Z.J. Ren, Microbial capacitive desalination for integrated organic matter and salt removal and energy production from unconventional natural gas produced water, Environ. Sci.-Water Res. Technol. 1 (1) (2015) 47–55, https://doi.org/10.1039/c4ew00050a.
[27] D. Zhang, F. Yang, T. Shimotori, K.-C. Wang, Y. Huang, Performance evaluation of power management systems in microbial fuel cell-based energy harvesting applications for driving small electronic devices, J. Power Sources 217 (2012) 65–71, https://doi.org/10.1016/j.jpowsour.2012.06.013.
[28] F. Yang, D. Zhang, T. Shimotori, K.-C. Wang, Y. Huang, Study of transformer-based power management system and its performance optimization for microbial fuel cells, J. Power Sources 205 (2012) 86–92, https://doi.org/10.1016/j.jpowsour.2012.01.025.
[29] K. Saravanakumar, R. Rajeswari, Microbial fuel cell-based self-powered biosensor for environment monitoring in IoT cloud framework, Concurr. Comput.-Pract. Exp. 31 (15) (2019), https://doi.org/10.1002/cpe.5165.
[30] T. Yamashita, T. Hayashi, H. Iwasaki, M. Awatsu, H. Yokoyama, Ultra-low-power energy harvester for microbial fuel cells and its application to environmental sensing and long-range wireless data transmission, J. Power Sources 430 (2019) 1–11, https://doi.org/10.1016/j.jpowsour.2019.04.120.
[31] M. Alaraj, J.-D. Park, Net power positive maximum power point tracking energy harvesting system for microbial fuel cell, J. Power Sources 418 (2019) 225–232, https://doi.org/10.1016/j.jpowsour.2019.02.042.
[32] F. Fischer, M. Sugnaux, C. Savy, G. Hugenin, Microbial fuel cell stack power to lithium battery stack: Pilot concept for scale up, Appl. Energy 230 (2018) 1633–1644, https://doi.org/10.1016/j.apenergy.2018.09.030.
[33] J. Yeo, T. Kim, J.K. Jang, Y. Yang, Practical maximum-power extraction in single microbial fuel cell by effective delivery through power management system, Energies 11 (9) (2018) Sep, https://doi.org/10.3390/en11092312.
[34] F. Khaled, O. Ondel, B. Allard, Microbial fuel cells as power supply of a low-power temperature sensor, J. Power Sources 306 (2016) 354–360, https://doi.org/10.1016/j.jpowsour.2015.12.040.
[35] Z. Ge, L. Wu, F. Zhang, Z. He, Energy extraction from a large-scale microbial fuel cell system treating municipal wastewater, J. Power Sources 297 (2015) 260–264, https://doi.org/10.1016/j.jpowsour.2015.07.105.
[36] X. Zhang, H. Ren, S. Pyo, J.-I. Lee, J. Kim, J. Chae, A high-efficiency DC-DC boost converter for a miniaturized microbial fuel cell, IEEE Trans. Power Electron. 30 (4) (2015) 2041–2049, https://doi.org/10.1109/TPEL.2014.2323075.
[37] N. Degrenne, et al., 'Self-Starting DC:DC Boost Converter for Low-Power and Low-Voltage Microbial Electric Generators', in 2011 IEEE ENERGY CONVERSION CONGRESS AND EXPOSITION (ECCE), in IEEE Energy Conversion Congress and Exposition, IEEE Power Elect Soc; IEEE Ind Applicat Soc, IEEE, 2011, pp. 889–896.
[38] F. Khaled, O. Ondel, B. Allard, Optimal energy harvesting from serially connected microbial fuel cells, IEEE Trans. Ind. Electron. 62 (6) (2015) 3508–3515, https://doi.org/10.1109/TIE.2014.2371437.
[39] J.-D. Park, Z. Ren, Hysteresis-controller-based energy harvesting scheme for microbial fuel cells with parallel operation capability, IEEE Trans. Energy Convers. 27 (3) (2012) 715–724, https://doi.org/10.1109/TEC.2012.2196044.
[40] C.-L. Nguyen, B. Tartakovsky, L. Woodward, Harvesting energy from multiple microbial fuel cells with a high-conversion efficiency power management system, ACS Omega 4 (21) (2019) 18978–18986, https://doi.org/10.1021/acsomega.9b01854.
[41] S. Carreon-Bautista, C. Erbay, A. Han, E. Sanchez-Sinencio, Power management system with integrated maximum power extraction algorithm for microbial fuel cells, IEEE Trans. Energy Convers. 30 (1) (2015) 262–272, https://doi.org/10.1109/TEC.2014.2352654.
[42] A. Costilla-Reyes, C. Erbay, S. Carreon-Bautista, A. Han, E. Sanchez-Sinencio, A time-interleave-based power management system with maximum power extraction and health protection algorithm for multiple microbial fuel cells for internet of things smart nodes, Appl. Sci.-Basel 8 (12) (2018) Dec, https://doi.org/10.3390/app8122404.
[43] B. Ringeisen, et al., High power density from a miniature microbial fuel cell using Shewanella oneidensis DSP10, Environ. Sci. Technol. 40 (8) (2006) 2629–2634, https://doi.org/10.1021/es052254w.
[44] C. Erbay, S. Carreon-Bautista, E. Sanchez-Sinencio, A. Han, High performance monolithic power management system with dynamic maximum power point tracking for microbial fuel cells, Environ. Sci. Technol. 48 (23) (2014) 13992–13999, https://doi.org/10.1021/es501426j.
[45] D. Molognoni, et al., Reducing start-up time and minimizing energy losses of microbial fuel cells using maximum power point tracking strategy, J. Power Sources 269 (2014) 403–411, https://doi.org/10.1016/j.jpowsour.2014.07.033.
[46] J.-D. Park, Z. Ren, High efficiency energy harvesting from microbial fuel cells using a synchronous boost converter, J. Power Sources 208 (2012) 322–327, https://doi.org/10.1016/j.jpowsour.2012.02.035.
[47] S. Carreon-Bautista, C. Erbay, A. Han, E. Sanchez-Sinencio, An inductorless DC–DC converter for an energy aware power management unit aimed at microbial fuel cell arrays, IEEE J. Emerg. Sel. Top. Power Electron. 3 (4) (2015) 1109–1121.

[48] M. Alaraj, M. Radenkovic, J.-D. Park, Intelligent energy harvesting scheme for microbial fuel cells: Maximum power point tracking and voltage overshoot avoidance, J. Power Sources 342 (2017) 726–732.
[49] D. Kashyap, et al., Application of electrochemical impedance spectroscopy in bio-fuel cell characterization: A review, Int. J. Hydrog. Energy 39 (35) (2014) 20159–20170, https://doi.org/10.1016/j.ijhydene.2014.10.003.
[50] C. Xia, D. Zhang, W. Pedrycz, Y. Zhu, Y. Guo, Models for microbial fuel cells: a critical review, J. Power Sources 373 (2018) 119–131, https://doi.org/10.1016/j.jpowsour.2017.11.001.
[51] H.C. Boghani, I. Michie, R.M. Dinsdale, A.J. Guwy, G.C. Premier, Control of microbial fuel cell voltage using a gain scheduling control strategy, J. Power Sources 322 (2016) 106–115, https://doi.org/10.1016/j.jpowsour.2016.05.017.